Article

Microseismic Monitoring of the Fracture Nucleation Mechanism and Early Warning for Cavern Rock Masses

Jin-Shuai Zhao [1,2], Yue-Mao Zhao [1,*], Peng-Xiang Li [3], Chong-Feng Chen [4], Jian-Cong Zhang [5] and Jiang-Hao Chen [2]

[1] College of Energy and Mining Engineering, Shandong University of Science and Technology, Qingdao 266590, China; jszhaomechanics@126.com

[2] Faculty of Civil Engineering and Mechanics, Jiangsu University, Zhenjiang 212013, China; 15189288482@163.com

[3] College of Urban Construction, Heze University, Heze 274015, China; lipengxiangsd@163.com

[4] Xi'an Research Institute, China Coal Technology and Engineering Group Corporation, Xi'an 710077, China; chenchongfeng@cctegxian.com

[5] PowerChina Huadong Engineering Corporation Limited, Hangzhou 311122, China; zhang_jc4@hdec.com

* Correspondence: zhaoyuemao@sdust.edu.cn

Abstract: The rock mass is susceptible to instability and damage during cavern construction. The blast-induced cracking process of the rock mass contains a wealth of information about the precursors of instability, and the identification of fracture nucleation signals is a prerequisite for effective hazard warning. A laboratory mechanical test and microseismic (MS) monitoring were carried out in the Baihetan Cavern to investigate the fracture nucleation process in the rock mass. MS monitoring shows that pre-existing microcracks were closed or new cracks were generated under the action of high stress, which caused the migration of microcracks. As the crack density increases, the fracture interaction gradually increases. The study of the rock fracture nucleation mechanism helps to reveal the MS sequences during the rock fracture process, and the fore-main shock was found in the MS sequence during access tunnel excavation. This study can effectively provide guidance for the early warning of rock mass failure and the stability analysis of underground caverns under blasting excavation disturbance.

Keywords: underground cavern; microseismic monitoring; fracture nucleation; early warning; stability analysis

1. Introduction

As underground engineering becomes deeper, excavation will inevitably lead to a certain degree of cracking or the local failure of surrounding rock [1–4]. To date, the main excavation mode of hard rock caverns is drill and blast [5–8]. Previous studies show that the microcracks of rock mass are excited under the action of blasting load, which results in damage deterioration or even ultimate local failure in underground caverns (Figure 1) [9–14]. These macroscopic failures of rock mass are largely attributed to the result of the evolution of internal cracks [15]. Unfortunately, the damage of rock mass is irreversible. When the degree of damage to the rock mass accumulates to the threshold, it is easy to induce rock mass instability failure under the action of blasting excavation disturbance [16]. In underground engineering, there is a contradiction between rock blasting excavation and the protection of the cavern, which must be solved [17–24]. From the viewpoint of cavern stability, it is essential to excavate the cavern in a rational manner using the blasting technique and to reduce the deterioration caused by rock damage.
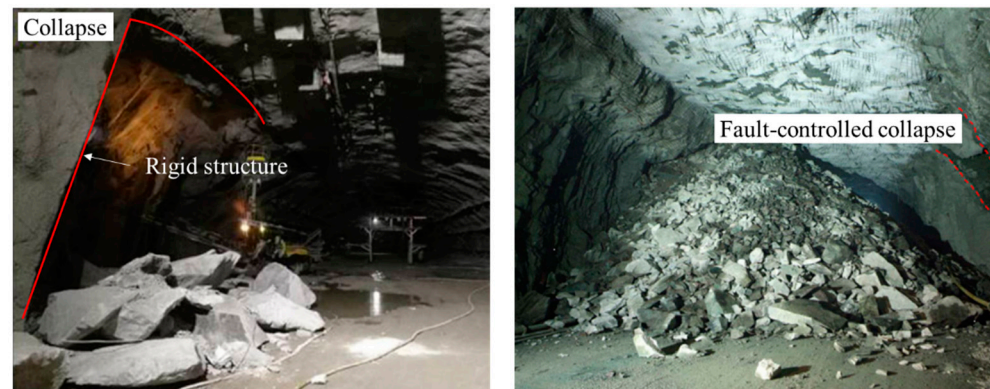
Figure 1. Severe rock failure cases of an underground cavern.

A proper assessment of rock mass damage and the nucleation mechanism induced by blasting excavation could provide guidance for the adjustment of subsequent construction. Theoretically, the evolution of cracks inside surrounding rock is a non-linear process [25–28]. There may be mutual influence and promotion between multiple cracks, and macroscopic failure is essentially the result of the accumulation of internal microcracks [29–33]. In the process of stress redistribution, it may induce internal fracture of the rock mass or shear dislocation along the original structural plane. The most commonly used in situ method for studying unloading fracture in underground rock engineering is MS monitoring [34–36]. The nucleation of cracks is initiated when the stress exceeds a certain threshold value [37–39].

In order to effectively reveal the cracking process and nucleation mechanism of macroscopic rock failure under blast load and to ensure the stability of the underground cavern, MS monitoring was implemented in the Baihetan Cavern. The internal microcrack evolution and cumulative damage mechanism of hard rock under blast load were intuitively revealed, which greatly enriches our understanding of the rock's mechanical behavior under blast disturbance.

2. Project Overview

2.1. Background

The layout of the caverns in the Baihetan project is shown in Figure 2. The caverns of the hydropower stations are arranged symmetrically in the mountains. The caverns consist of the powerhouse, tailrace gate room, main transformer room, tailrace surge tank, and drainage tunnels. The hydroelectric project is equipped with 16 sets of hydro-generator units independently developed by China, with a single unit capacity of 1000 MW. The significance of the sustainable development of the Baihetan hydropower station is that the annual power generation can meet the demand of about 75 million people, which can replace about 19.68 million tons of burning coal and reduce about 52 million tons of carbon dioxide emissions.

2.2. Network Topology of the Microseismic System

The MS monitoring system consists of a server, modem, DSL modem, UPS, net ADC, net SP, and uniaxial geophones (Figure 3). The designed sampling frequency of the MS monitoring system is 6000 Hz. The principle of signal acquisition is that the released elastic waves induced by rock fractures are detected by the MS sensors and then the wave signals are transferred to the net ADC. These signals are then converted into digital signals. Finally, the digital signals can be processed into rock fracture earthquake spectra. These earthquake spectra are transferred to the server and then the experienced microseismic engineer can process the MS signals in the monitoring center at the Baihetan office.
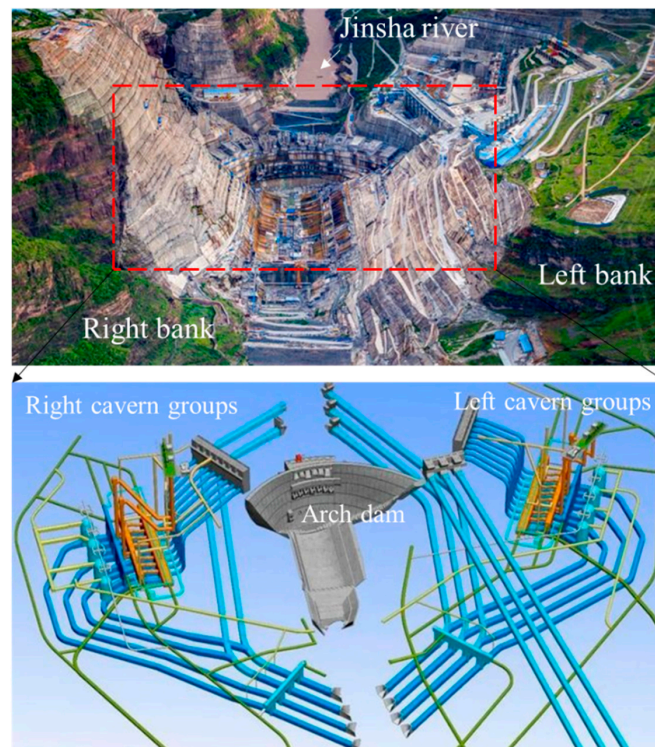
Figure 2. The layout of caverns in the Baihetan project.


Figure 3. Components and communication mode of the MS system.

The spatial arrangement of MS sensors in the study area of the caverns is displayed in Figure 4. A total of three monitoring sections were arranged in the study area, and two sensors were installed in each monitoring section. The distance between each monitoring section is 30 m. The six sensors (No. 29~No. 34) used in the field are uniaxial geophones. The parameters of the geophones are listed in Table 1. The valid MS sensor array is fundamental to the study of the fracture process. According to the MS location algorithm, the fracture signal monitored by four or more sensors can be effectively located. In this study, six sensors were used to monitor the fracture process of the rock mass. The number of sensors is more than four, which can effectively ensure the continuity and accuracy of the MS monitoring results.
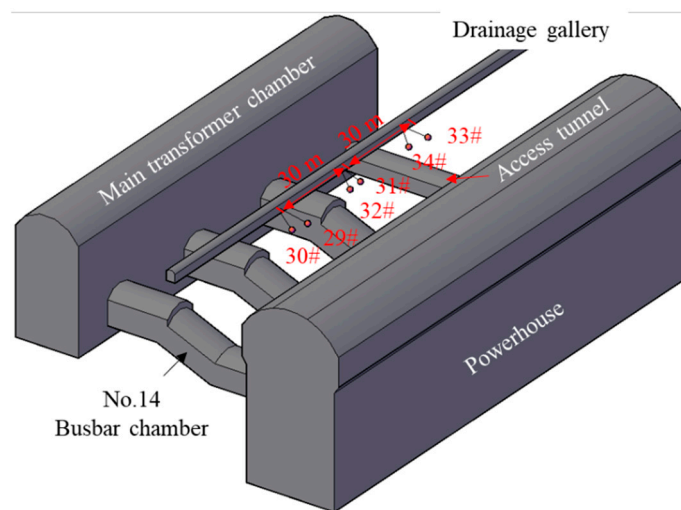
Figure 4. Arrangement of MS sensors in the study area of the underground caverns.

In addition, preventive measures were also proposed to prevent the destruction of the array and to protect the continuity of the MS data. Firstly, borehole and grouting technology was used to install the MS sensor. Coupling of the MS sensor and the surrounding rock can significantly enhance the quality of the captured MS data. Secondly, a steel pipe is inserted into the surrounding rock to safeguard the exposed communication cable (Figure 5). Engineering practices have proved that these preventive measures effectively guarantee the reliability of the MS data.
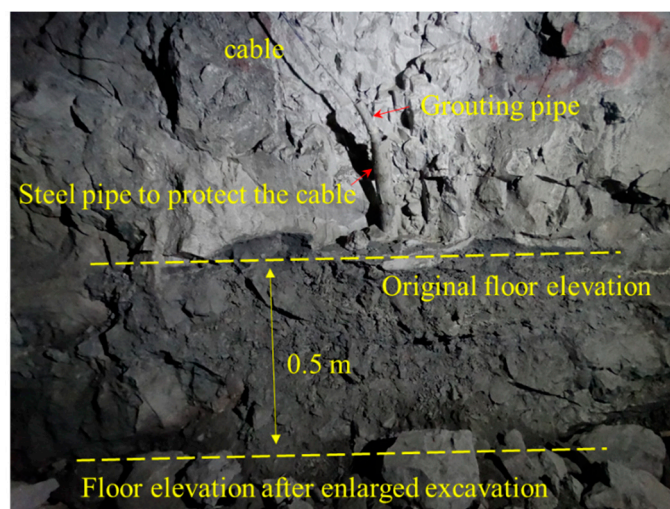

Figure 5. The procedure used to safeguard the MS sensor array.

Table 1. Parameters of microseismic geophones.

Sensor	Orientation	Natural Frequency	Response Range
Geophone	Uniaxial	10 Hz	10~2000 Hz

2.3. Study Area

The access tunnel of the underground cavern was selected as the test site to monitor the crack process of the rock mass, and the selected study area is demonstrated in Figure 6. The range of the study area is 60 m wide surrounding the access tunnel.
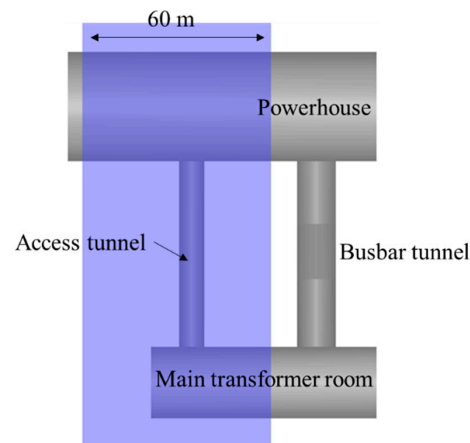
Figure 6. Survey region of MS monitoring of the rock crack process in caverns.

3. Fracture Nucleation Mechanism

3.1. Laboratory Test

Scholars have carried out systematic research work on rock cracking and have a deeper understanding of rock damage and deformation processes [40–43]. During rock uniaxial compression, the axial and lateral strains were measured by an axial extensometer and circumferential strain gauge, respectively. Then, the total volumetric strain of the rock sample can be calculated as:

$$\varepsilon_v = \varepsilon_1 + 2\varepsilon_3 \tag{1}$$

where ε_1 is the axial strain and ε_3 is the lateral strain. The Poisson's ratio v and elastic modulus E are calculated by the linear elastic section of the stress–strain curve. According to the three principal stresses σ_1, σ_2, σ_3 of the rock sample, the elastic volumetric strain caused by the deformation of the rock matrix under different stress states is calculated as:

$$\varepsilon_v^e = \frac{1 - 2v}{E}(\sigma_1 + \sigma_2 + \sigma_3) \tag{2}$$

The volume deformation of the rock samples is influenced by the rock matrix and microcracks. For uniaxial compression ($\sigma_2 = \sigma_3 = 0$), the volumetric strain caused by micropores and microcracks in the rock is:

$$\varepsilon_v^c = \varepsilon_v - \varepsilon_v^e = \varepsilon_v - \frac{1 - 2v}{E}\sigma_1 \tag{3}$$

There are four stress thresholds in the rock failure process: (1) closure stress σ_{cc} of initial microcracks; (2) initiation stress σ_{ci} of new microcracks; (3) damage stress σ_{cd}; and (4) peak stress σ_p, also denoted as for uniaxial compressive strength σ_c. Once the damage stress is exceeded, the crack density increases greatly. Strain softening occurs in brittle rock, resulting in irreversible crack damage [44]. The damage stress corresponds to the long-term strength of the rock sample [45].

The internal cracking of rock is very complex and the measurement of characteristic stresses, such as initiation stress, damage stress, and peak stress, can represent the state of the rock. However, acoustic emission and MS contain rich information about cracks, and the internal damage and cracking process of the rock can be revealed by analyzing the characteristics of the seismic signals.

3.2. In Situ Microseismic Monitoring

3.2.1. Evolution of MS Activity with Time

During the fracture process of the rock, the inelastic seismic wave is radiated outwards, which is recorded as an MS event after being captured by the MS sensors. Theoretically, a rupture of rock mass will produce an MS event. Figure 7 demonstrates the temporal evolution of MS events with time in the access tunnel. It is clear that MS events accumulated rapidly in the rock mass from 1 to 16 August 2016. And the number of MS events increased slowly from 17 August to 12 September 2016. Then, the MS activity characteristics of the rock mass were in a calm state. Finally, the number of MS events increased rapidly in the rock mass from 13 to 19 September 2016. MS events are closely related to the internal fracture of the rock mass, which directly reflects the evolution characteristics of the inside cracks of the rock mass.
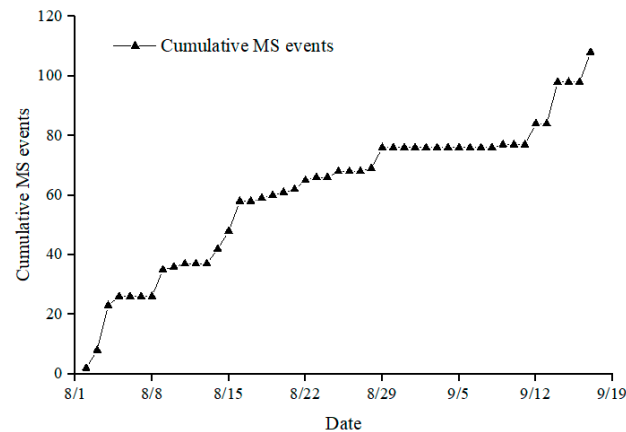
Figure 7. Time evolution of cumulative MS events during excavation.

The distribution characteristics of MS events with different moment magnitudes induced by blasting excavation are shown in Figure 8. The moment magnitude of MS events ranges from -3.0 to -0.5 and is concentrated in the range of $(-2.0, -1.0)$, which reveals that the region meets the seismic conditions for possible rock mass failure.
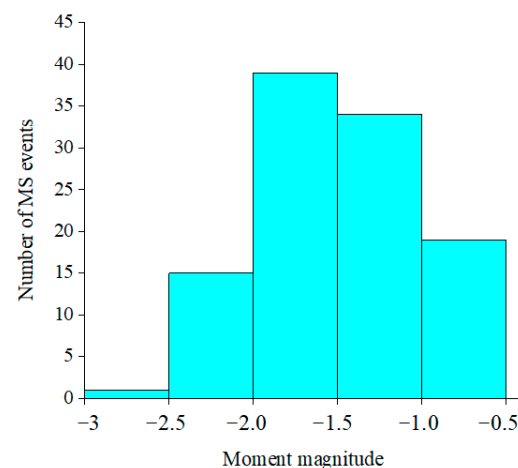
Figure 8. Statistics of MS events with different moment magnitudes.

3.2.2. Spatial Distribution of MS Activity

The spatial evolution of MS events is shown in Figure 9. The fractures of rock mass in the access tunnel are excited by blasting disturbance. The micro-fractures of the rock mass are randomly initiated. The adjacent micro-fractures are far away from each other, and the interaction of micro-fractures is weak. The pre-existing microcracks close or new cracks are generated under the action of high stress, which leads to the migration of microcracks. With the increase in crack density, the interaction of fractures is gradually enhanced, and the micro-fracture changes from disorder to order. When the local density of the micro-fracture reaches the critical value, local nucleation of the micro-fracture occurs. In the later stage of micro-fracture evolution, nucleation reaches the macro-scale and finally leads to the nucleation of small-scale micro-fractures into large-scale cracks or faults. The blasting-induced MS events are clustered in the roof of the access tunnel, and the corresponding spalling failure is shown in Figure 10. Once the fracture nucleation forms a local weakening of the macroscopic critical scale, it will lead to the instability and failure of the rock mass.
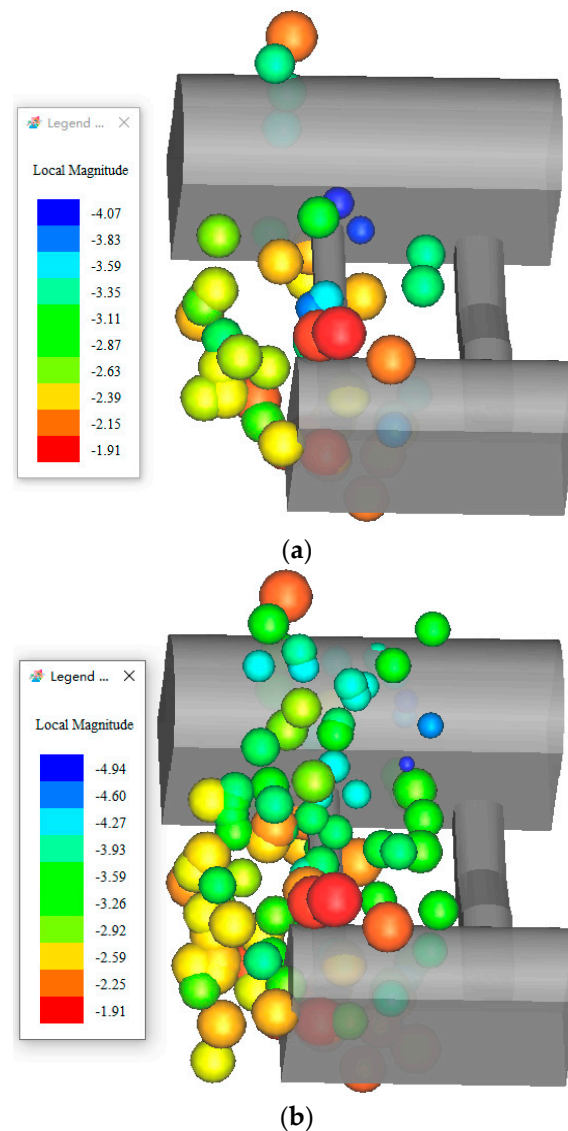
Figure 9. Spatial distribution of blasting-induced MS events. (**a**) Initiation of rock fracture and (**b**) nucleation of rock fracture.

Figure 10. Blasting-induced spalling failure of rock mass in the access tunnel.

3.2.3. Macroscopic Damage Risk Warning

In the field of seismology, the forecast of rock failure can be based on a statistical approach in the short and long term [46]. There is no doubt that more information can be obtained through long-term monitoring and that the effect of the early warning will be more precise. The evolution curves of energy index (*EI*) and cumulative apparent volume with time can reflect the micro-fracture characteristics before the macroscopic failure of rock mass and evaluate the stability of the cavern. The computational formula of *EI* is:

$$EI = \frac{E}{\overline{E}(P)} \tag{4}$$

In the formula, *EI* is the energy index and $\overline{E}(P)$ is the average released MS energy in the analysis area.

The energy index and cumulative apparent volume evolution curve induced by blasting excavation are shown in Figure 11. From 5 to 23 August 2016, the energy index showed an overall upward trend, while the cumulative apparent volume increased slowly. The MS deformation of rock mass in this period was small, and the surrounding rock was in the compaction stage before the peak strength of the rock. From 24 to 30 August 2016, the energy index decreased rapidly in a stepped manner, and the cumulative apparent volume increased rapidly, indicating that the stored strain energy of the rock mass exceeded the limited storage capacity. The rapid release of energy in the source, accompanied by an increase in the inelastic deformation volume, indicates that the risk of macroscopic deformation or fracture is increasing. At this time, an early warning should be issued in time. From 31 August to 10 September 2016, the energy index and cumulative apparent volume showed an upward trend. Similarly, if no timely support reinforcement measures or insufficient support strength were taken after the previous stage of early warning, the risk of macroscopic failure of rock mass at this stage was greater. In short, before the macroscopic failure of the rock mass occurs, it has the remarkable characteristics of a sudden increase in apparent volume and a sudden decrease in energy index. Combined with the temporal and spatial evolution law of MS events, it can be seen that the MS events in the access tunnels induced by blasting excavation increase rapidly, which indicates that the risk of surrounding rock fracture is high. The failure characteristics of the surrounding rock of the access tunnel further verify the accuracy of risk early warning results based on MS parameters.
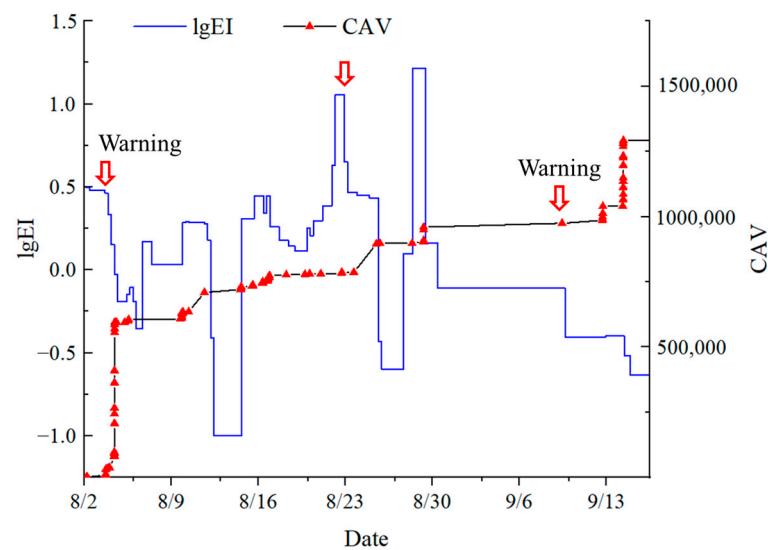
Figure 11. Evolution of energy index (*EI*) and cumulative apparent volume (CAV) induced by blasting excavation.

4. Discussion

4.1. MS Sequences

The crack evolution and nucleation mechanism are related to the characteristics of the rock medium. The study of the rock fracture nucleation mechanism helps to reveal the MS sequences during the rock fracture process. Mogi [47] studied the failure of different rock materials in acoustic emission experiments. (1) In homogeneous rock, the number of microcracks before the main crack is very small. However, there are many microcracks after the main crack. (2) In heterogeneous rock materials, a large number of microcracks occur before and after the main crack. (3) It is worth noting that in the failure process of extremely heterogeneous rock materials, there are many microcracks, but there is no main crack. Based on the above observations of different rock mediums, three types of AE sequences are summarized: main shock sequence, fore-main shock sequence, and swarm shock sequence.

In fact, there are many MS events with different energies during the fracturing process of the rock mass. The maximum energy of an MS event is $10^2 \sim 10^4$ times that of the minimum energy. The role of MS events with low energy is almost ignored in the MS energy evolution curve. In order to avoid the influence of order of magnitude difference, the radiated energy of ith MS event is processed by finding the cube root as follows:

$$E_i^* = \sqrt[3]{E_i} \tag{5}$$

Then, to compare the characteristic between the AE sequence and MS sequence induced by blasting disturbance, the evolution curves of moment magnitude and cumulative energy in the MS sequence is shown in Figure 12. The MS energy is processed by the cube root transformation. In this study, the evolution characteristics of microseismicity in Figure 12 is the fore-main shock MS sequence. Engineering practices have proved that the fracture process of rock mass macroscopic failure has two remarkable characteristics [48]. The first feature is the random generation of internal cracks of rock, which is also the accumulation period of damage degradation. The seismic events of this period correspond to the foreshock of the MS sequence. The second feature is the generation and evolution of rock cracks gradually changed from disorder to order, contributing to the fracture merging and nucleation of rock mass. In the meantime, the number and scale of cracks accelerate and enter the unstable failure stage. The seismic events of this period correspond to the main shock of the MS sequence.
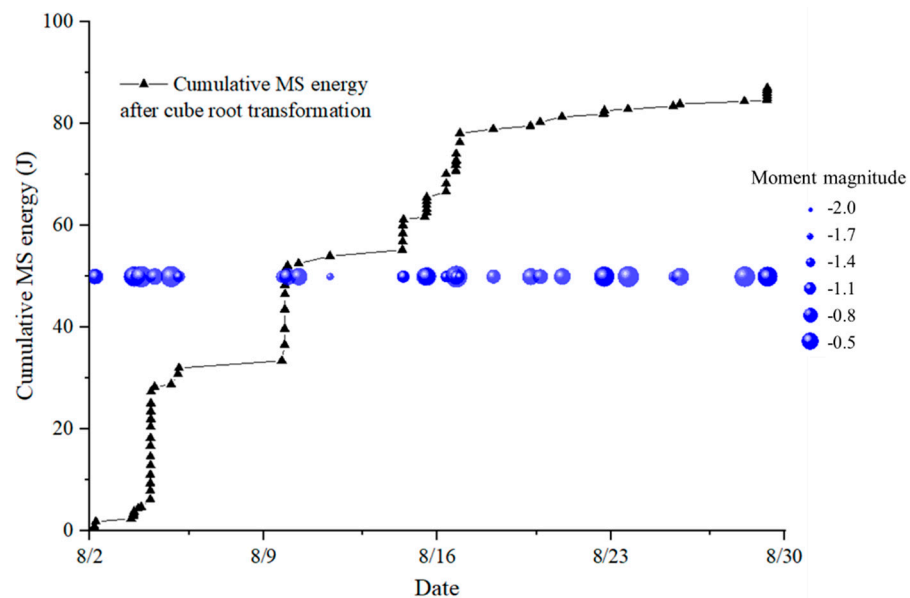
Figure 12. Evolution curves of moment magnitude and cumulative energy in the MS sequence.

4.2. Kinetic Model

Microseismology is derived from earthquake seismology. The common kinetic model of seismology is also used in the field of microseismology. The kinetic mode can help us to understand the mechanical behavior and the destruction process of the rock mass. The determination of the fracture mechanism and source parameters is based on the well-known kinetic model of the Brune model [49]. The Brune model assumes that the seismic source is a circular dislocation and that the instantaneous stress drop is generated along the dislocation. The Brune model was developed by Madariaga [50], who modified the concept of the source radius. In the Madariaga model, the seismic source is considered to be an extended circular crack with a finite rupture velocity. The size of the crack plays a very important role in the process of fracture nucleation in the rock mass. The source radius can be used to characterize the size of the rock fracture in the underground cavern. The source radius is calculated on the basis of the velocity of the S-wave and the corner frequency as follows:

$$r = \frac{cV_S}{2\pi f_0} \tag{6}$$

In the formula, r is the source radius; c is a constant and the value of c depends on the source model; Vs is the S-wave velocity; and f_0 is the corner frequency.

For the Brune and Madariaga models, the constant c is 2.34 and 1.32, respectively. This means that the calculated fracture size of the Brune model is twice that of the Madariaga model. The magnitude of the rock mass rupture induced by the earthquake is large. The Brune model assumes that the source is a double couple shear mechanism, so the model has a wide range of applications in earthquake engineering. However, in underground caverns, the excavation-induced fracture is relatively small, and the source is dominated by the tensile mechanism. The size calculated by the Brune model is significantly larger than the fracture size observed in the field. Relatively speaking, the size calculated by the Madariaga model is closer to engineering practice. Therefore, the study of a kinetic model suitable for the tensile fracture mechanism of underground caverns is of great benefit to fully reveal the destruction process of the rock mass. The next stage of research is to study a kinetic model suitable for underground caverns and to test the effectiveness of the model.

5. Conclusions

An MS monitoring technique was implemented to study the blasting-induced fracture nucleation mechanism of rock mass in underground caverns. It is clearly shown that inside

cracking in laboratory rock is very complicated and that simply measuring the peak stress does not reflect the cracking process. That is, it is momentous to explore the internal crack and damage process of the rock mass, which can be used for warning about the macroscopic instability of surrounding rock.

By analyzing the characteristics of the seismic signals radiated by rock cracking, the fracture nucleation of rock masses can be comprehensively revealed. The MS monitoring results show that the micro-fractures of rock mass are randomly initiated. With the increase in crack density, the interaction of fractures is gradually enhanced, and micro-fracture changes from disorder to order. When the fracture nucleation forms a local weakening of the macroscopic critical scale, it will lead to the instability and failure of caverns. The MS energy index and cumulative apparent volume evolution curve can be used for early warning of the failure of the rock mass.

References

1. Hoek, E.; Brown, T. *Underground Excavation in Rock*; The Institute of Mining and Metallurgy: London, UK, 1980.
2. Yang, K.; Wang, L.; Ge, J.; He, J.; Sun, T.; Wang, X.; Zhao, Y. Impact of formation dip angle and wellbore azimuth on fracture propagation for shale reservoir. *Processes* **2023**, *11*, 2419. [CrossRef]
3. Gong, F.Q.; Yan, J.Y.; Li, X.B.; Luo, S. A peak-strength strain energy storage index for bursting proneness of rock materials. *Int. J. Rock Mech. Min. Sci.* **2019**, *117*, 76–89. [CrossRef]
4. Xu, D.; Liu, X.; Jiang, Q.; Li, S.; Zhou, Y.; Qiu, S.; Yan, F.; Zheng, H.; Huang, X. A local homogenization approach for simulating the reinforcement effect of the fully grouted bolt in deep underground openings. *Int. J. Min. Sci. Technol.* **2022**, *32*, 247–259. [CrossRef]
5. Konicek, P.; Soucek, K.; Stas, L.; Singh, R. Long-hole destress blasting for rockburst control during deep underground coal mining. *Int. J. Rock Mech. Min. Sci.* **2013**, *61*, 141–153. [CrossRef]
6. Yan, P.; Zhao, Z.G.; Lu, W.B.; Fan, Y.; Chen, X.R.; Shan, Z.G. Mitigation of rock burst events by blasting techniques during deep-tunnel excavation. *Eng. Geol.* **2015**, *188*, 126–136. [CrossRef]
7. Zhao, J.-S.; Chen, B.-R.; Jiang, Q.; Lu, J.-F.; Hao, X.-J.; Pei, S.-F.; Wang, F. Microseismic monitoring of rock mass fracture response to blasting excavation of large underground caverns under high geostress. *Rock Mech. Rock Eng.* **2022**, *55*, 733–750. [CrossRef]
8. Fan, Y.; Lu, W.B.; Zhou, Y.H.; Yan, P.; Leng, Z.D.; Chen, M. Influence of tunneling methods on the strainburst characteristics during the excavation of deep rock masses. *Eng. Geol.* **2016**, *201*, 85–95. [CrossRef]
9. Li, A.; Dai, F.; Wu, W.; Liu, Y.; Liu, K.; Wang, K. Deformation characteristics of sidewall and anchorage mechanisms of prestressed cables in layered rock strata dipping steeply into the inner space of underground powerhouse cavern. *Int. J. Rock Mech. Min. Sci.* **2022**, *159*, 105234. [CrossRef]
10. Zhao, J.S.; Jiang, Q.; Pei, S.F.; Chen, B.R.; Xu, D.P.; Song, L.B. Microseismicity and focal mechanism of blasting-induced block falling of intersecting chamber of large underground cavern under high geo-stress. *J. Cent. South Univ.* **2023**, *30*, 542–554. [CrossRef]
11. Li, B.; Ding, Q.; Xu, N.; Lei, Y.; Xu, Y.; Zhu, Z.; Liu, J. Mechanical response and stability analysis of rock mass in high geostress underground powerhouse caverns subjected to excavation. *J. Cent. South Univ.* **2020**, *27*, 2971–2984. [CrossRef]
12. Tang, Y.; Okubo, S.; Xu, J.; Peng, S. Progressive failure behaviors and crack evolution of rocks under triaxial compression by 3D digital image correlation. *Eng. Geol.* **2019**, *249*, 172–185. [CrossRef]
13. Zheng, Z.; Cai, Z.; Su, G.; Huang, S.; Wang, W.; Zhang, Q.; Wang, Y. A new fractional-order model for time-dependent damage of rock under true triaxial stresses. *Int. J. Damage Mech.* **2022**, *32*, 50–72. [CrossRef]
14. Xu, H.; Li, S.; Xu, D.; Huang, X.; Zheng, M.; He, J.; Zhao, K. Numerical back analysis method of three-dimensional in situ stress fields considering complex surface topography and variable collinearity. *Int. J. Rock Mech. Min. Sci.* **2023**, *170*, 105474. [CrossRef]

15. Cai, M. Principles of rock support in burst-prone ground. *Tunn. Undergr. Space Technol.* **2013**, *36*, 46–56. [CrossRef]
16. Ma, T.H.; Tang, C.A.; Tang, L.X.; Zhang, W.D.; Wang, L. Rockburst characteristics and microseismic monitoring of deep-buried tunnels for Jinping II hydropower station. *Tunn. Undergr. Space Technol.* **2015**, *49*, 345–368. [CrossRef]
17. Zhao, J.; Feng, X.; Jiang, Q.; Zhou, Y. Microseismicity monitoring and failure mechanism analysis of rock masses with weak interlayer zone in underground intersecting chambers: A case study from the Baihetan hydropower station, China. *Eng. Geol.* **2018**, *245*, 44–60. [CrossRef]
18. Li, P.X.; Chen, B.R.; Xiao, Y.X.; Feng, G.L.; Zhou, Y.Y.; Zhao, J.S. Rockburst and microseismic activity in a lagging tunnel as the spacing between twin TBM excavated tunnels changes: A case from the Neelum-Jhelum hydropower project. *Tunn. Undergr. Space Technol.* **2023**, *132*, 104884. [CrossRef]
19. Zhang, C.Q.; Feng, X.T.; Zhou, H.; Qiu, S.L.; Wu, W.P. A top pilot tunnel preconditioning method for the prevention of extremely intense rockbursts in deep tunnels excavated by TBMs. *Rock Mech. Rock Eng.* **2012**, *45*, 289–309. [CrossRef]
20. Dai, F.; Li, B.; Xu, N.W.; Fan, Y.L.; Zhang, C.Q. Deformation forecasting and stability analysis of large-scale underground powerhouse caverns from microseismic monitoring. *Int. J. Rock Mech. Min. Sci.* **2016**, *86*, 269–281. [CrossRef]
21. Liu, F.; Tang, C.A.; Ma, T.H.; Tang, L.X. Characterizing rockbursts along a structural plane in a tunnel of the Hanjiang-to-Weihe river diversion project by microseismic monitoring. *Rock Mech. Rock Eng.* **2019**, *52*, 1835–1856. [CrossRef]
22. Cao, A.Y.; Dou, L.M.; Wang, C.B.; Yao, X.X.; Dong, J.Y.; Gu, Y. Microseismic precursory characteristics of rock burst hazard in mining areas near a large residual coal pillar: A case study from Xuzhuang coal mine, Xuzhou, China. *Rock Mech. Rock Eng.* **2016**, *49*, 4407–4422. [CrossRef]
23. Mazaira, A.; Konicek, P. Intense rockburst impacts in deep underground construction and their prevention. *Can. Geotech. J.* **2015**, *52*, 1426–1439. [CrossRef]
24. Xu, H.; Xu, D.; Li, S.; Zheng, M.; Huang, X.; Chen, B.; Feng, G.; Xu, Y. Stress tensor similarity index based on Euclidean distance for numerical back analysis of in situ stress fields. *Comput. Geotech.* **2023**, *159*, 105457. [CrossRef]
25. Li, Z.-W.; Long, M.-C.; Xu, P.; Huang, C.-Y.; Wang, Y.-S. Thermal contact resistance of granite joints under normal stress. *Rock Mech. Rock. Eng.* **2023**, online. [CrossRef]
26. Li, Z.-W.; Huang, C.-Y.; Wang, H.-X.; Xing, S.-C.; Long, M.-C.; Liu, Y. Determination of heat transfer representative element volume and three-dimensional thermal conductivity tensor of fractured rock masses. *Int. J. Rock Mech. Min. Sci.* **2023**, *170*, 105528. [CrossRef]
27. Barton, N.; Lien, R.; Lunde, J. Engineering classification of rock masses for the design of tunnel support. *Rock Mech.* **1974**, *6*, 189–236. [CrossRef]
28. Feng, F.; Chen, S.; Wang, Y.; Huang, W.; Han, Z. Cracking mechanism and strength criteria evaluation of granite affected by intermediate principal stresses subjected to unloading stress state. *Int. J. Rock Mech. Min. Sci.* **2021**, *143*, 10473. [CrossRef]
29. Chen, S.; Feng, F.; Wang, Y.; Li, D.; Huang, W.; Zhao, X.; Jiang, N. Tunnel failure in hard rock with multiple weak planes due to excavation unloading of in-situ stress. *J. Cent. South Univ.* **2020**, *27*, 2864–2882. [CrossRef]
30. Zhang, B.; Wang, L.; Liu, J. Effect of fracture geometry parameters on the permeability of a random three-dimensional fracture network. *Processes* **2023**, *11*, 2237. [CrossRef]
31. Feng, F.; Chen, S.; Han, Z.; Golsanami, N.; Liang, P.; Xie, Z. Influence of moisture content and intermediate principal stress on cracking behavior of sandstone subjected to true triaxial unloading conditions. *Eng. Fract. Mech.* **2023**, *284*, 109265. [CrossRef]
32. Kumar, V.; Gopalakrishnan, N.; Singh, N.P.; Cherukuri, S. Microseismic monitoring application for primary stability evaluation of the powerhouse of the Tapovan Vishnugad Hydropower Project. *J. Earth. Syst. Sci.* **2019**, *128*, 169. [CrossRef]
33. Cook, N.G.W.; Hoek, E.; Pretorius, J.P.G.; Ortlepp, W.D.; Salamon, M.D.G. Rock mechanics applied to the study of rockbursts. *J. South Afr. Inst. Min. Metall.* **1966**, *66*, 435–528.
34. Tang, Z.L.; Liu, X.L.; Xu, Q.J.; Li, C.Y.; Qin, P.X. Stability evaluation of deep-buried TBM construction tunnel based on microseismic monitoring technology. *Tunn. Undergr. Space Technol.* **2018**, *81*, 512–524. [CrossRef]
35. Chen, B.-R.; Feng, X.-T.; Li, Q.-P.; Luo, R.-Z.; Li, S.-J. Rock burst intensity classification based on the radiated energy with damage intensity at Jinping II Hydropower Station, China. *Rock Mech. Rock Eng.* **2015**, *48*, 289–303. [CrossRef]
36. Xu, N.W.; Li, T.B.; Dai, F.; Li, B.; Zhu, Y.G.; Yang, D.S. Microseismic monitoring and stability evaluation for the large scale underground caverns at the Houziyan hydropower station in Southwest China. *Eng. Geol.* **2015**, *188*, 48–67. [CrossRef]
37. Zhao, J.S.; Jiang, Q.; Lu, J.F.; Chen, B.R.; Pei, S.F.; Wang, Z.L. Rock fracturing observation based on microseismic monitoring and borehole imaging: In situ investigation in a large underground cavern under high geo-stress. *Tunn. Undergr. Space Technol.* **2022**, *126*, 104549. [CrossRef]
38. Li, F.; Cheng, Y.; Zhang, X.; Huang, S.; Li, D. Change characteristics of the advance stress and strata fracture structure of spatial isolated island formed by roof drainage. *Processes* **2023**, *11*, 246. [CrossRef]
39. Zheng, Z.; Tang, H.; Zhang, Q.; Pan, P.; Zhang, X.; Mei, G.; Liu, Z.; Wang, W. True triaxial test and PFC3D-GBM simulation study on mechanical properties and fracture evolution mechanisms of rock under high stresses. *Comput. Geotech.* **2023**, *154*, 105136. [CrossRef]
40. Hudyma, M.; Potvin, Y.H. An engineering approach to seismic risk management in hardrock mines. *Rock Mech. Rock Eng.* **2009**, *43*, 891–906. [CrossRef]
41. Zheng, Z.; Su, H.; Mei, G.; Wang, W.; Liu, H.; Zhang, Q.; Wang, Y. A thermodynamic damage model for 3D stress-induced mechanical characteristics and brittle–ductile transition of rock. *Int. J. Damage Mech.* **2023**, *32*, 623–648. [CrossRef]

42. Zhou, J.; Li, X.B.; Mitri, H.S. Evaluation method of rockburst: State-of-the-art literature review. *Tunn. Undergr. Space Technol.* **2018**, *81*, 632–659. [CrossRef]

43. Hoek, E.; Martin, C.D. Fracture initiation and propagation in intact rock—A review. *J. Rock Mech. Geotech. Eng.* **2014**, *6*, 287–300. [CrossRef]

44. Martin, C.D.; Chandler, N.A. The progressive fracture of Lac du Bonnet granite. *Int. J. Rock Mech. Min. Sci. Geomech. Abstr.* **1994**, *31*, 643–659. [CrossRef]

45. Bieniawski, Z.T. Mechanism of brittle fracture of rock, Parts II and III. *Int. J. Rock Mech. Min. Sci. Geomech. Abstr.* **1967**, *4*, 395–430. [CrossRef]

46. Mendecki, A.J. *Seismic Monitoring in Mines*; Chapman & Hall: London, UK, 1997.

47. Mogi, K. Study of elastic shocks caused by the fracture of heterogonous materials, and its relation to the earthquake phenomena. *Bull. Earth. Res. Inst.* **1962**, *40*, 125–173.

48. Kuksenko, V.; Tomilin, N.; Damaskinskaya, E.; Lockner, D. A two-stage model of fracture of rocks. *Pure. Appl. Geophys.* **1996**, *146*, 253–263. [CrossRef]

49. Brune, J. Tectonic stress and the spectra of seismic shear waves from earthquakes. *J. Geophys. Res.* **1970**, *75*, 4997–5009. [CrossRef]

50. Madariaga, R. Dynamics of an expanding circular fault. *Bull. Seismol. Soc. Am.* **1976**, *66*, 639–666. [CrossRef]